(Received 13 June 2025, Accepted 5 August 2025, Scheduled 9 September 2025)

Improved Low Sidelobe Pattern Synthesis of Planar Arrays having a Distorted Triangular or Rectangular Lattice due to Row Displacements

Will P. M. N. Keizer[1,*]

[1] *retired, before working with The Physics Laboratory TNO, Oud Waalsdorperweg 63, 2597 AK, The Hague, The Netherlands*

ABSTRACT: This paper describes how the low sidelobe pattern synthesis of planar arrays with a distorted triangular or rectangular lattice, caused by row displacements, can be improved using the iterative Fourier transform (IFT) method. Array antennas with a rectangular or triangular lattice combined with row displacements have an array factor that lacks periodicity in cosine u-v space for the u-direction. This means that for the u-direction, the pattern synthesis using the IFT method is limited to far-field directions that belong to the rectangular sector of the array factor computed by the inverse 2D FFT. Missing far-field directions in the pattern synthesis occur when the width of the computed array factor (AF) in u-v space is < 2. In this case, not all far-field directions in visible u-v space are engaged in the pattern synthesis. The solution to this problem is to reduce the inter-element spacing along the rows with a factor two by including dummy elements with zero excitation between the active elements in each row. In this way, the width of AF, computed by the inverse 2D FFT, is doubled in u-v space. This doubling will result in twice as many far-field directions in the u-direction being involved in the pattern synthesis. After successful synthesis, all dummy excitations are removed from the synthesized set of excitations. The element excitations thus obtained, without the dummy ones, still perform the same as the original excitation obtained from the pattern synthesis. Three examples will demonstrate the validity of this solution.

1. INTRODUCTION

A recent paper [1] describes the use of the IFT method for the low sidelobe pattern synthesis of planar arrays with a rectangular or triangular element lattice in combination with row displacements. The described pattern synthesis results apply to three different array configurations with displaced rows. The IFT synthesis used requires a peak sidelobe level (PSLL) of ≤ -50 dB for the near-in sidelobes all positioned in a nulling ring sector and a PSLL of ≤ -68 dB for the far-out sidelobes in a second nulling ring sector. The third array configuration in [1] must meet the same requirements, including a nulling rectangular sector with a ≤ -80 dB PSLL.

The described synthesized results are almost in line with the user's requirements, except for a very few far-field directions located at the second null ring sector with a PSLL requirement of ≤ -68 dB. For these few directions, their PSLL is about a few dB higher than the specified ≤ -68 dB. The reason for these slightly higher PSLL's are the row displacements of the three array configurations. Row displacements not only cut the double periodicity of the aperture element lattice, but therefore also the double periodicity of AF in the cosine u-v space. Only for the v-direction of u-v space, AF retains its periodicity. The absence of periodicity in the u-direction of AF restricts the low sidelobe pattern synthesis with the IFT method to u-directions of the far-field within the rectangular sector of the AF as calculated by the inverse 2D FFT described in [2].

* Corresponding author: Will P. M. N. Keizer (willkeizer@ieee.org).

In all three examples in [1], the AF computed with the IFT method, has a width wAF < 2 in the u-direction of u-v space. Due to this width, all far-field directions with |u|> wAF/2 are excluded from the IFT synthesis of low side lobe patterns. Therefore, some of these far-field positions in the sidelobe region of AF violate the PSLL ≤ -68 dB requirement by a few dB. All three examples in [1] suffer from this shortcoming. In this paper a simple solution is presented that overcomes this shortcoming of the IFT method when applied to array antennas having a rectangular or triangular element lattice in combination with displaced rows. The effectiveness of the simple solution is proven with the re-synthesis of the same three examples as in [1].

2. DISTORTED TRIANGULAR OR RECTANGULAR LATTICE

Figure 1 shows the element locations of a planar array aperture having a triangular element lattice. All odd numbered rows feature the same displacement $\Delta_n = 0.5$ while for the even numbered rows Δ_n is equal to $\Delta_n = 0$. The elements in the same row have an inter-element spacing of d_x. The vertical spacing between two successive rows is d_y. The equation of AF in u-v space valid for the triangular lattice of Fig. 1 is given by

$$F(u,v) = \sum_{m=0}^{M-1} \sum_{n=0}^{N-1} A_{mn} e^{jk[(m+\Delta_n)d_x u + n d_y v]} \quad (1)$$

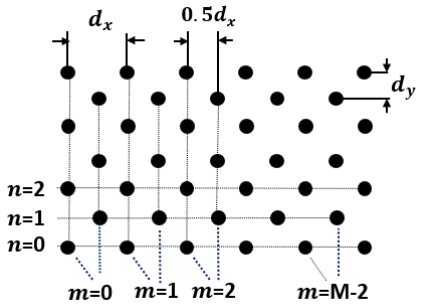

FIGURE 1. Triangular element lattice (originally published in [1]).

$$\Delta_n = 0.5 \text{ for } n = \text{odd}, \Delta_n = 0 \text{ for } n = \text{even or } 0$$

where A_{mn} is the excitation of element (m, n), k the wavenumber $(2\pi/\lambda)$, and λ the wavelength. In (1) u and v are the direction cosines $u = \sin\theta\cos\varphi$ and $v = \sin\theta\sin\varphi$ with θ the elevation angle.

When the row displacement in Fig. 1 for every row is equal to $\Delta_n = 0$, the triangular lattice becomes a rectangular one. A skew lattice is obtained when the row displacement varies accordance to $\Delta_n = n*\text{del}$ with del in the range of $-1 < \text{del} < 1$. The preceding part of Section 2, including Fig. 1 and Equation (1), is replicated from [1].

In [1] the results of three low sidelobe pattern synthesis examples are presented for array configurations with array apertures which have row displacements in combination with a rectangular or triangular lattice. Due to these row displacements, the results of used IFT synthesis do not fully match the applied low sidelobe design requirements. This paper repeats the low sidelobe pattern synthesis of the three examples in [1] with the same low sidelobe design requirements but applies a simple correction to remove the negative PSLL impact of the row displacement on the synthesized AF using the IFT method.

2.1. Periodicity of AF

The synthesis of low sidelobe pattern used in this paper is the same IFT method as described in [1] and is based on the application of the newly developed couple of inverse and forward 2D FFTs described in [2]. These new 2D FFT formulations are an essential part of the IFT method used in [1], but also in this paper.

The array factor *AFuv* calculated by the inverse 2D FFT of [2] for u-v space always has a rectangular shape with a width of λ/d_x in the u-direction and a height of λ/d_y in the v-direction. The u-v coordinates of *AFuv* are in the range

$$-\frac{\lambda}{2d_x} \le u \le \frac{\lambda}{2d_x} \tag{2}$$

$$-\frac{\lambda}{2d_y} \le v \le \frac{\lambda}{2d_y} \tag{3}$$

see [1]. The pattern synthesis performed with any IFT method focuses exclusively on the far-field distribution in *AFuv*. This is not a limitation as long as the *AFuv* has a double periodicity, which is the case when the element lattice is rectangular, triangular or skewed. In these three cases, *AFuv* repeats itself in u-v space in two directions and the pattern synthesis can therefore be restricted to *AFuv*.

Due to the row displacements of the three examples in [1], their calculated *AFuv*'s are only periodic in the v-direction and not in the u-direction. Furthermore, these *AFuv*'s do not cover entire visible u-v space in the u-direction, with the result that not the entire visible far-field distribution participates in the pattern synthesis. Fig. 2 shows the sector of *AFuv* of the first two examples of [1] in u-v space. For these examples, the element spacing d_x along each row is equal to 0.018 m and the spacing d_y between two successive rows is also equal to 0.018 m. The operating frequency is 10 GHz. From Fig. 2 it can be seen that *AFuv* of these two examples does not cover entire visible u-v space in the u-direction nor in the v-direction. This is related to the size of d_x and d_y at 10 GHz, (2) and (3). Due to the row displacements *AFuv* misses in the u-direction periodicity but not in the v-direction. The missing periodicity in the u-direction, is the reason that *AFuv* lacks replicas in that direction. Only in the v-direction does *AFuv* repeat itself, as can be seen from the green colored replicas below and above *AFuv*. The same problem applies also to the third example of [1] which again shows row displacements in combination with an *AFuv* that in the u-direction does not cover entire visible u-v space because the spacing between two consecutive elements $d_x > 0.5\lambda$.

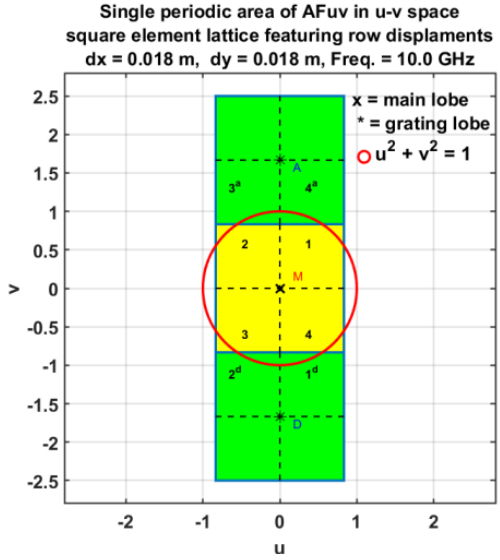

FIGURE 2. Sector of the single periodic region of *AFuv* (yellow rectangle) in u-v space at 10 GHz. The green colored square blocks are copies of *AFuv* due to its periodicity in the v-direction. No replicas of *AFuv* in the u-direction. The main beam is positioned at broadside. This figure refers to the *AFuv* of Examples 1 and 2, described in [1].

2.2. Solution for the Missing Periodicity of AF in u-Direction

The absence of double periodicity for *AFuv* has degraded the IFT synthesis for all three examples in [1] since not all far-out sidelobes matches the ≤ -68 dB PSLL requirement. The reason for this shortcoming is the lack of periodicity in the u-direction combined with an *AFuv* with a width smaller than 2. This limitation can be easily eliminated by adding a dummy element with zero amplitude between two consecutive active elements of each row. Such an addition reduces the spacing d_x

between the elements of each row with a factor two and therefore doubles the width of *AFuv* in u-v space, (2). The spacing between two consecutive rows d_y is kept constant. The impact of the reduction of d_x by a factor 2 at 10 GHz on the sector of *AFuv* in the u- direction of u-v space is shown in Fig. 3. The result of this doubling of the width of *AFuv* means that its area will cover entire visible u-v space in the u-direction. By using a modified array configuration equipped with dummy elements and keeping the excitation of the dummy elements zero during each iteration of the IFT synthesis, the impact of the single periodicity of *AFuv* on the PSLL performance can be mitigated. After successful pattern synthesis, all dummy excitations are then removed from the synthesized set of excitations. The resulting element excitations without the dummy excitations are therefore suitable for the original aperture and still perform exactly as the original synthesized excitations with the dummy elements. This simple solution has been successfully applied to all three examples of [1] as will be demonstrated.

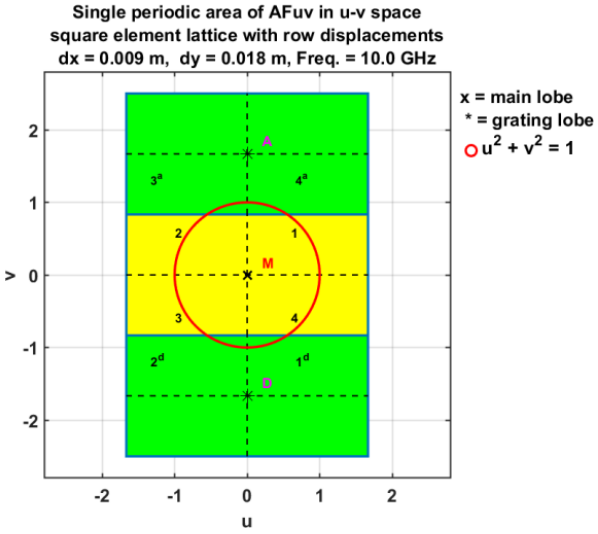

FIGURE 3. Single periodic region of *AFuv* (yellow rectangle) at 10 GHz in u-v space. This *AFuv* applies when the d_x spacing between adjacent elements of the first two examples of [1] is reduced to 0.009 m and the original spacing between two successive rows is kept. The green colored rectangular blocks are copies of *AFuv* due to its periodicity in the v-direction. No replicas of *AFuv* in the u-direction. The main beam is positioned at broadside. This figure refers to the *AFuv* sector in u-v space of Examples 1 and 2 in this paper.

3. IMPROVED RESULTS FOR THE THREE EXAMPLES OF [1]

In this section the renewed synthesis of the low sidelobe pattern is discussed, applied to the three examples in [1]. The purpose of these redesigns is to reduce the limited number of far-out sidelobes for u-directions with $|u| > 0.833$, which do not match the applied PSLL requirements. The redesign of the pattern synthesis applied to the three examples of [1] is based on the use of dummy elements in the way described in the previous section. The redesigned pattern synthesis is for the first two examples conducted with the amplitude-only condition for the element excitations. For the renewed synthesis of Example 3, the condition of complex amplitude is applied to the elements.

3.1. Resynthesis Low Sidelobe Pattern Example 1

The aperture element layout of the array of the first example in [1] is shown in Fig. 4. The elements of the array antenna are situated along 22 rows and 22 columns according to a square lattice with $d_x = d_y = 0.018$ m. Only the bottom and top row are displaced to the right over a distance of 0.009 m. Fig. 5 shows the synthesized AF at 10 GHz obtained with the original IFT method applied to the original aperture of Fig. 4 and presented in [1]. It can be seen that only for a small number of far-out sidelobes, with $|u| > 0.8333$, the PSLL specification of ≤ -68 dB is violated. The pattern synthesis performed for Example 1, as described in [1], is repeated for the modified aperture layout with 43 columns instead of the original 22 and 22 rows. Due to the almost double number of columns, the spacing d_x between the elements along each row is reduced to 0.009 m while the spacing d_y between two successive rows remains 0.018 m. This array aperture has the same size as the original aperture of Fig. 4 but contains 43×22 elements of which 462 elements are dummies with zero amplitude excitation for the entire duration of the synthesis. The pattern synthesis frequency used is 10 GHz, identical to that of the first example in [1]. The PSLL requirements used for the modified array aperture are almost the same as those applied for Example 1 in [1]. The requirement for the first nulling ring sector is identical: a PSLL of < -50 dB, its inner ring coincides with the first nulls of the main lobe, and its outer ring having a radius equal to 0.4. The outer ring of the second nulling ring sector has a radius of 1.38 instead of the original 1.18 and its inner ring coincides with the outer ring of the first nulling ring sector. By specifying 1.38 for the radius of the outer ring of sector 2, this nulling ring sector extends into invisible u-v space, which means that all sidelobes in visible u-v space participate in the resynthesis of the low sidelobe pattern using the IFT method. The region of *AFuv* in u-v space at 10 GHz, which refers to the modified array antenna with 47 columns and 22 rows, corresponds to the yellow rectangle shown in Fig. 3.

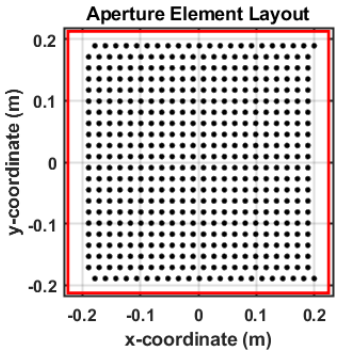

FIGURE 4. Positions of the array aperture element, showing the deformed square lattice with two displaced rows, one at the bottom and one at the top. Example 1 of [1].

Using the modified aperture layout, the pattern synthesis for Example 1 of [1], applied to its sum pattern is repeated with the

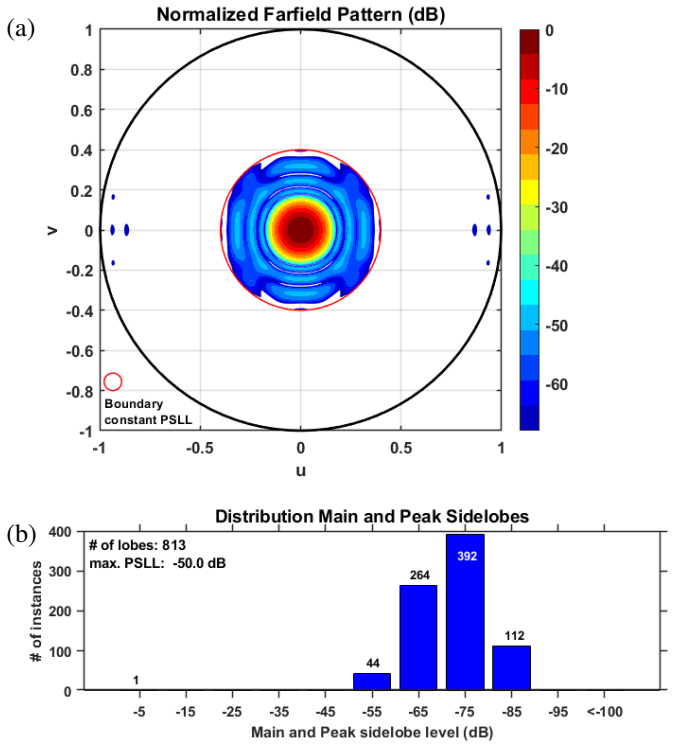

FIGURE 5. (a) Pseudo contour plot of the normalized array factor of the synthesized sum pattern. (b) Corresponding peak sidelobe level distribution for entire visible u-v space. Refer to Example 1 in [1].

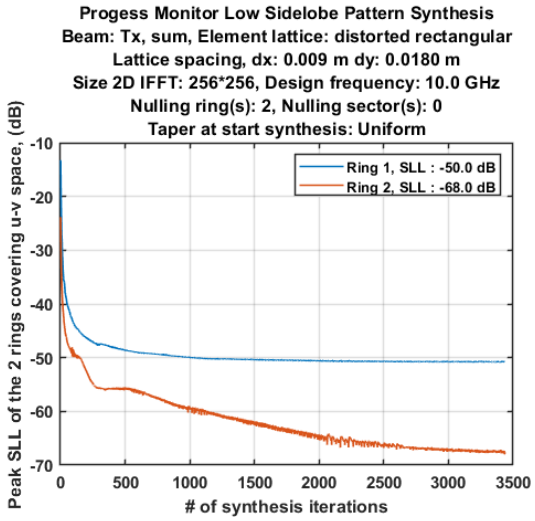

FIGURE 6. Convergence rate of the renewed low sidelobe synthesis of the sum pattern using the IFT method applied to the modified aperture layout with 552 dummy elements. Example 1 of this paper.

goal that all far-out sidelobes in visible u-v space have to match a < -68 dB PSLL at 10 GHz. Due to the doubling of elements along each row from 22 to 43, applied to the modified aperture layout, the original size of both 2D FFT's, inverse and forward, used by the IFT method during the renewed pattern synthesis, must be increased from 128×128 to 256×256. Fig. 6 shows the convergence rate of the low sidelobe pattern synthesis.

The redesigned IFT synthesis required 3436 iterations and matches all design requirements, as can be seen from Fig. 7(a).

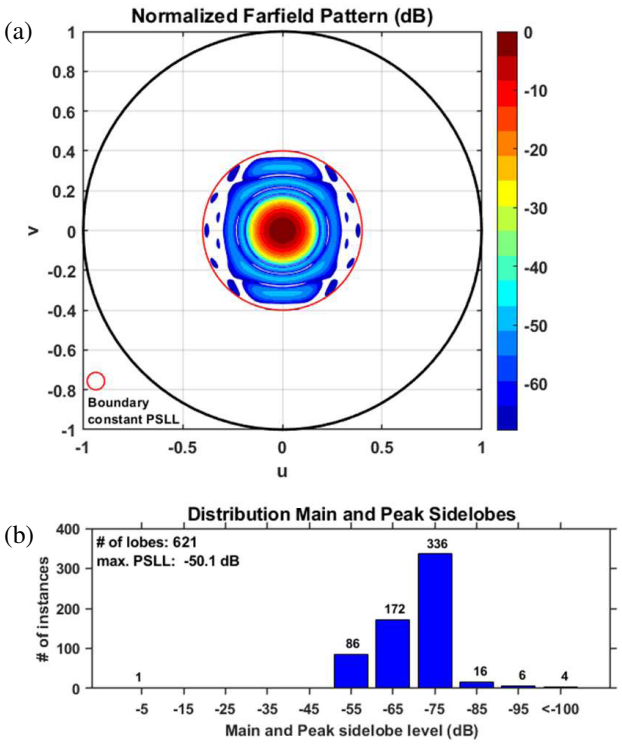

FIGURE 7. (a) Pseudo contour plot of the normalized array factor of the synthesized sum pattern. (b) Corresponding peak sidelobe level distribution for entire visible u-v space. Refer to Example 1 of this paper.

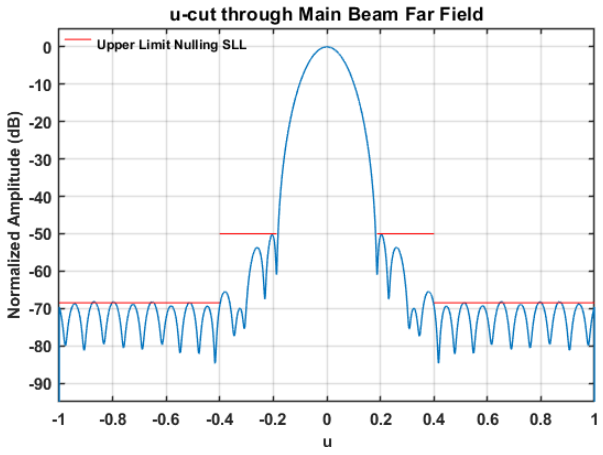

FIGURE 8. Principal u-cut of the array factor pattern shown in Fig. 7(a).

The normalized AF, shown in this figure, is produced by the synthesized excitations after removal of the 462 dummy values (zero amplitude excitations) and then applied to the original aperture layout shown in Fig. 4. As can be seen, the PSLL requirement is fully met for the second nulling ring sector. Figs. 8 and 9 show the u-cut and v-cut for the principal planes of the AF shown in Fig. 7(a). From Figs. 8 and 9, it can be seen that the PSLL requirement of < -50 dB is also fully met for the nulling ring sector 1.

The computation time for the redesign of the pattern synthesis of Example 1 was 6.7 seconds for 3436 iterations. The pattern synthesis of Example 1 in [1] required 1432 iterations

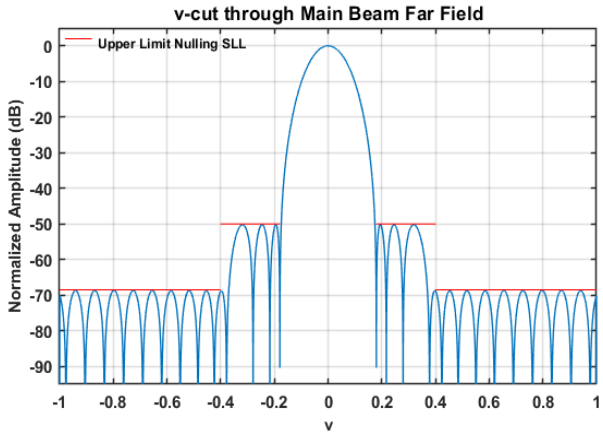

FIGURE 9. Principal v-cut of the array factor pattern shown in Fig. 7(a). Example 1 of this paper.

and the computation time was 0.99 seconds. The reason for the much larger computation time for the redesign of Example 1 is the 256×256 size of the 2D FFTs, inverse and forward, for the redesign instead of the size of 128×128 for the original design, due to the addition of 462 dummy elements whose amplitude must be kept at a zero during each iteration.

3.2. Resynthesis Low Sidelobe Pattern Example 2

Also, Example 2 in [1] does not meet all prescribed design specifications for the same reason as Example 1 of [1]. Fig. 10 shows the aperture layout used for Example 2 in [1]. With this layout six rows are displaced to the left over distance of 0.009 m. These displacements affect rows 1, 3, 5, 7, 9, and 11. The aperture has 24 columns and the same number of rows. The spacings d_x and d_y are both equal to 0.018 m. Without the displacement of the six rows, the aperture lattice is of the square type. The sector of *AFuv* in u-v space at 10 GHz, which corresponds to the layout of Fig. 10, is shown in Fig. 3.

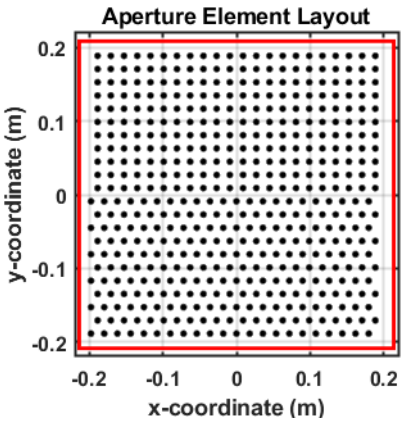

FIGURE 10. Positions of the array aperture element showing the deformed triangular/rectangular lattice. Example 2 in [1].

The redesign of the pattern synthesis of Example 2 in [1] to remove the limited number of far-out sidelobes, which exceed the PSLL requirement of ≤ -68 dB, follows the same route as applied for Example 1. The synthesis of the low sidelobe pattern of Example 2 in [1] involved two nulling ring sectors. Ring sector 1 has an outer radius equal to 0.45, while the inner ring of this sector must coincide with the null positions of the main lobe. The PSLL requirement for the nulling ring sector 1 is ≤ -50 dB and for ring sector 2 the PSLL is ≤ -68 dB. The outer ring radius of ring sector 2 was specified as 1.18 for the original pattern synthesis of Example 2 but is increased to 1.4 for the redesign of Example 2. The redesigned pattern synthesis of Example 2, which refers to the sum pattern, follows the same route as just described for the redesign of Example 1. The number of dummy elements is again equal to 462 due to the reduction of the row element spacing with a factor 2. The renewed IFT synthesis required 1922 iterations, matches all design requirements as shown in Fig. 11 and required a computation time of 3.2 seconds. The original pattern synthesis described in [1] for Example 2 needed 717 iterations and involved 0.43 seconds computation time.

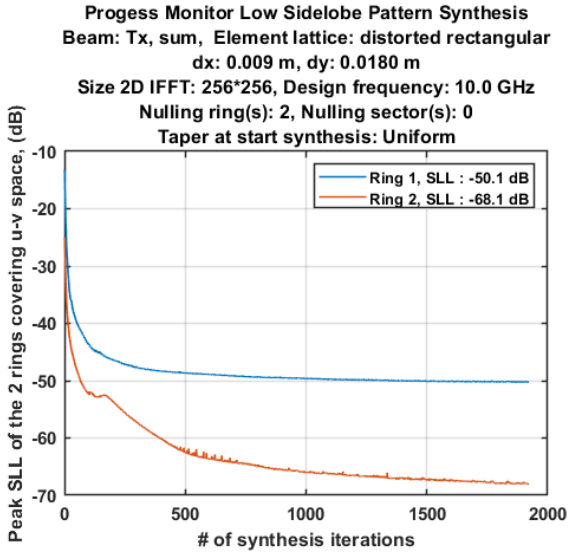

FIGURE 11. Convergence rate of the renewed synthesis of the low sidelobe sum pattern using the IFT method applied to the modified aperture layout with 484 dummy elements. Example 2 of this paper.

The normalized AF corresponding to the resynthesized element excitations after removing the dummy excitations and then applied to the original element layout of Fig. 10, is shown in Fig. 12(a), together with the distribution of the peak side lobe levels in Fig. 12(b). It can be seen that in entire visible u-v space no sidelobes of the nulling ring sector 1 exceed -50 dB PSLL and also, nor do any sidelobe of the nulling Sector 2 exceed the PSLL ≤ -68 dB requirement as shown in Figs. 13 and 14.

3.3. Resynthesis Low Sidelobe Pattern Example 3

Figure 15 shows the aperture layout of Example 3 described in [1]. All rows of this example are quasi-randomly displaced. Without the horizontal row displacements, the original element lattice is a triangular one. The array aperture has 640 elements distributed over 20 columns and 32 rows. The spacing between two neighboring elements on the same row $d_x = 0.020$ m and the spacing between the rows is $d_y = 0.0125$ m. The largest horizontal row displacement is 0.0526 m, and the minimum value is -0.0405 m.

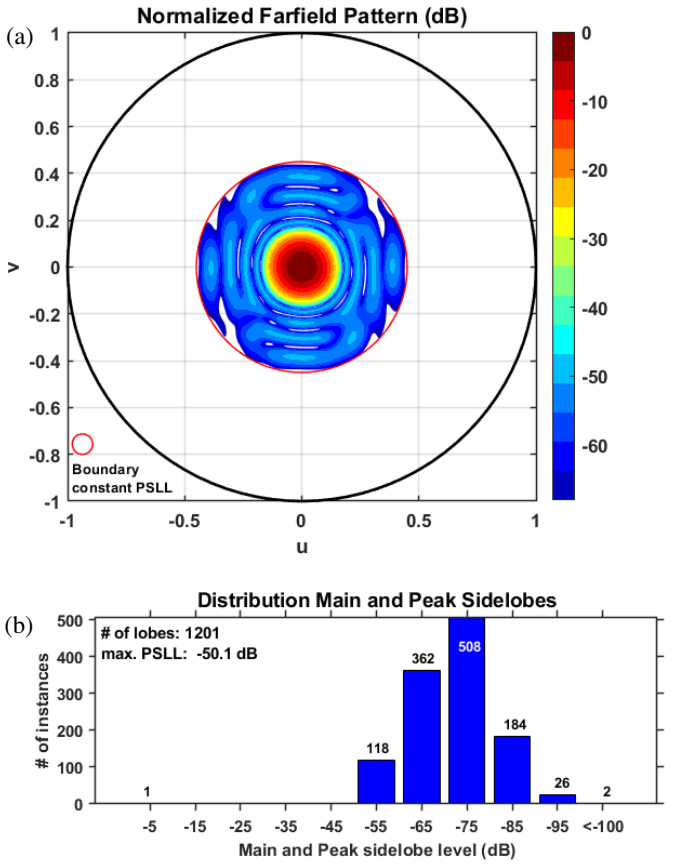

FIGURE 12. (a) Pseudo contour plot of the normalized array factor of the synthesized sum pattern. (b) Corresponding peak sidelobe level distribution for entire visible u-v space. Refers to Example 2 of this paper.

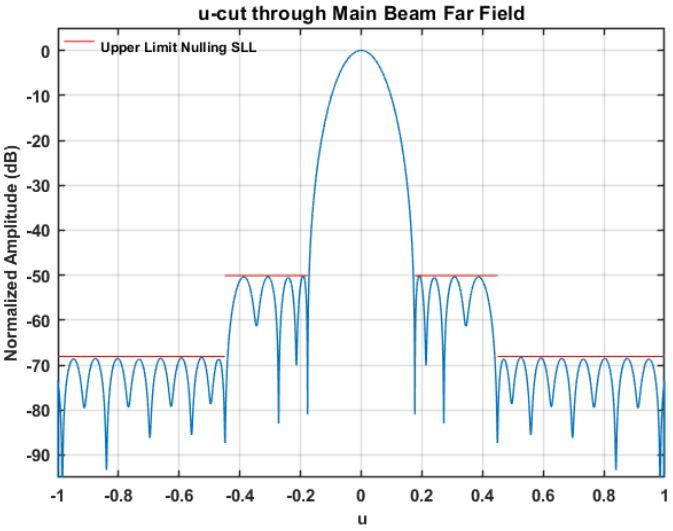

FIGURE 13. Principal u-cut of the array factor pattern shown in Fig. 12(a). Example 2 of this paper.

The low sidelobe synthesis for u-v space includes two nulling ring sectors with different PSLL requirements. The outer ring of ring sector 1 has a radius equal to 0.50, while its inner ring coincides with the null boundary of the main lobe. The PSLL requirement for ring sector 1 is ≤ -50 dB. The nulling ring sector

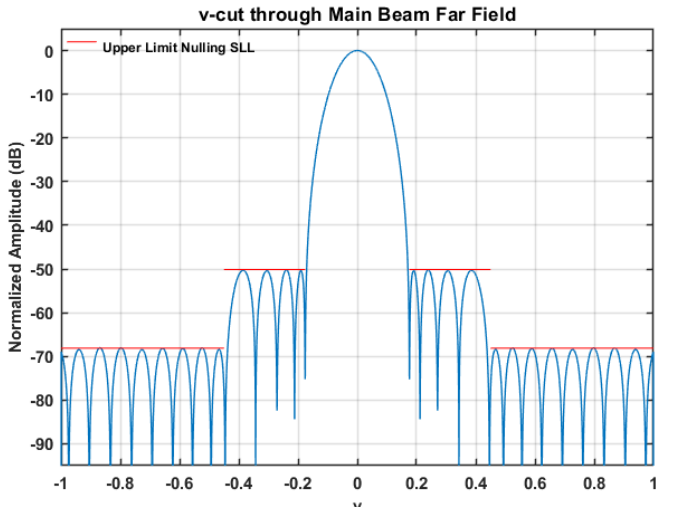

FIGURE 14. Principal v-cut of the array factor pattern shown in Fig. 12(a). Example 2 of this paper.

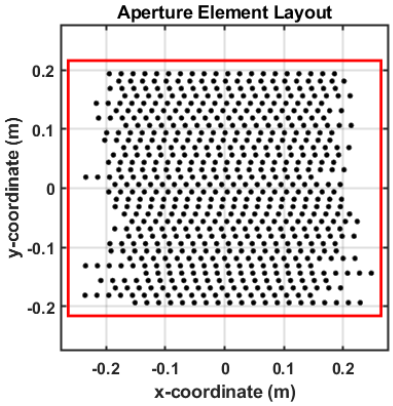

FIGURE 15. Positions of array aperture element showing the distorted triangular/rectangular lattice due to the random, variable horizontal row displacements. Example 3.

2 contains all u-v directions of the rectangular, single periodic *AFuv* except those of ring sector 1 and the ones of the main lobe. Also, for Example 3, the PSLL for nulling ring sector 2 is specified as ≤ -68 dB. The low sidelobe synthesis also includes a nulling rectangular sector, specified by $\{0.6 \leq u \leq 0.68$, and $-0.1 \leq v \leq 0.3\}$ with a PSLL specification equal to ≤ -80 dB.

For the redesign of Example 3, the spacing between two adjacent elements along each row is reduced by a factor 2 by adding 608 dummy elements with a zero amplitude during the resynthesis, in the same way as was done for the redesign of Examples 1 and 2. In addition, the radius of the outer ring of the nulling ring sector 2 is increased to 1.30. Fig. 16 shows the convergence rate of the resynthesis of the low sidelobe pattern of Example 3, in which resynthesis concerns the sum pattern. This resynthesis 3 involved 8800 iterations, which required 15.4 seconds of computation time.

Figure 17 shows the resynthesis of the low sidelobe pattern of Example 3 by the IFT method applied to the modified aperture layout, which includes 608 dummy elements with zero amplitude values. This result applies to the resynthesized element

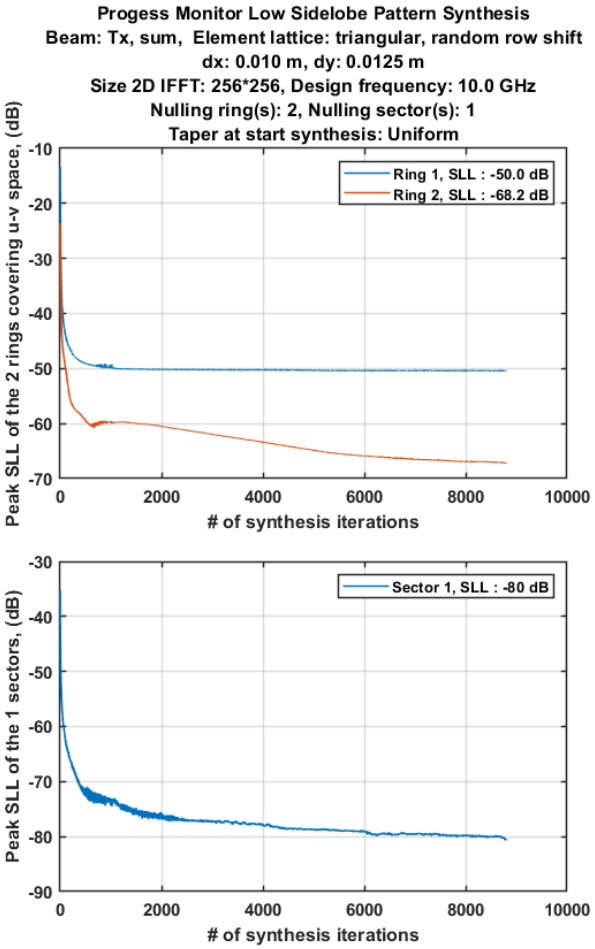

FIGURE 16. Convergence rate of the resynthesis of the low sidelobe sum pattern using the IFT method applied to the modified aperture layout with 552 dummy elements. These data refer to Example 3 of this paper.

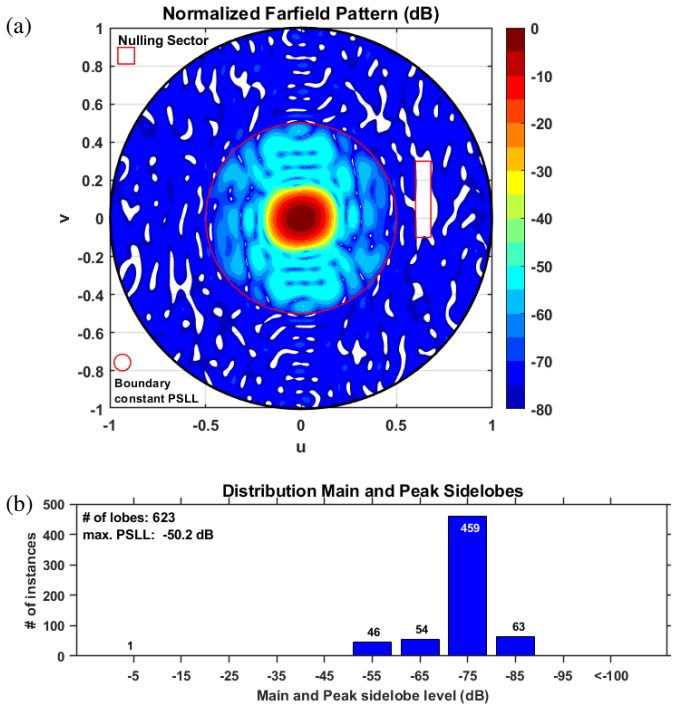

FIGURE 17. (a) Pseudo contour plot of the normalized array factor of the synthesized sum pattern. (b) Corresponding peak sidelobe level distribution for whole visible u-v space. Refer to Example 3 in this paper.

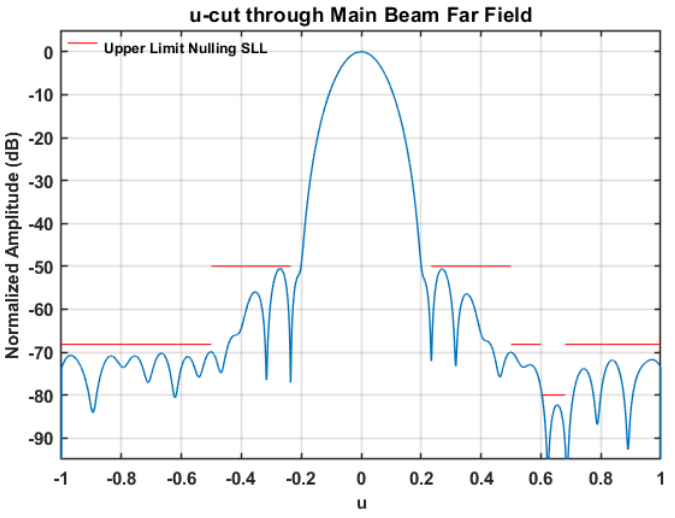

FIGURE 18. Principal u-cut of the array factor pattern shown in Fig. 17(a). Example 3 of this paper.

excitations applied to the layout shown in Fig. 15 after removing all zero amplitude dummy values.

The principal u- and v-cuts of the AF, shown in Fig. 17(a), are presented in Figs. 18 and 19, respectively. These three figures show that none of the three PSLL requirements for the sidelobe region are violated. In Fig. 20 where the main beam is scanned to the position $\theta = 80°$, $\varphi = 130°$ various parasitic grating lobes are visible however with lower peak values compared to the peak of the scanned main lobe. The two degenerated grating lobes visible for the u-range > 0.86 have a PSLL of -6.5 dB.

4. PARASITIC GRATING LOBES DUE TO ROW DISPLACEMENTS

The row displacements applied with the three reported examples in this paper create parasitic grating lobes that are located in invisible u-v space when the main beam is pointing at broadside. The number of these parasitic grating lobes depends on the number of displaced rows. Fig. 21 shows AF of Example 1 published in [1] for the range $\{-2 < u < 2, -2 < v < 2\}$. Fig. 22 does this for the resynthesized Example 1 of this paper. Figs. 23–24 do the same for the original and resynthesized Example 2 and Figs. 25–26 apply to both types of Example 3.

It can be noticed that row displacements create parasitic grating lobes. More row displacements result in more parasitic grating lobes. Figs. 22, 24 and 26 clearly show that for the nulling ring sector 2 of which outer ring extends completely in invisible u-v space, none of its sidelobes exceed the PSLL of -68 dB. The position of the outer ring of the ring sector 2 is indicated in Figs. 22, 24 and 26, by the black circle. These results illustrate ones again the effectiveness of the applied simple solution

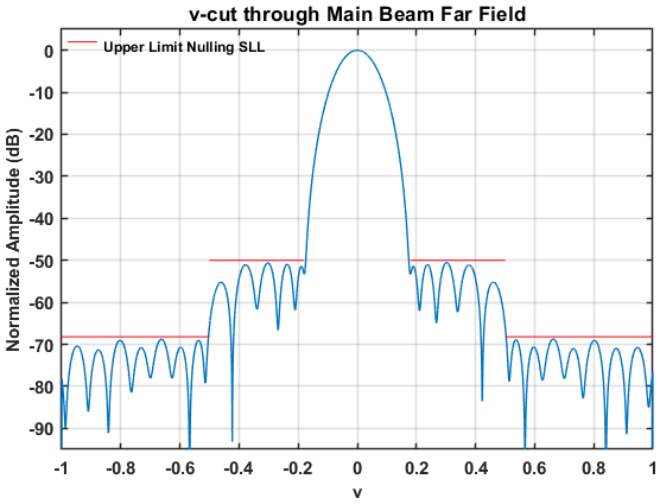

FIGURE 19. Principal v-cut of the array factor pattern shown in Fig. 17(a). Example 3 of this paper.

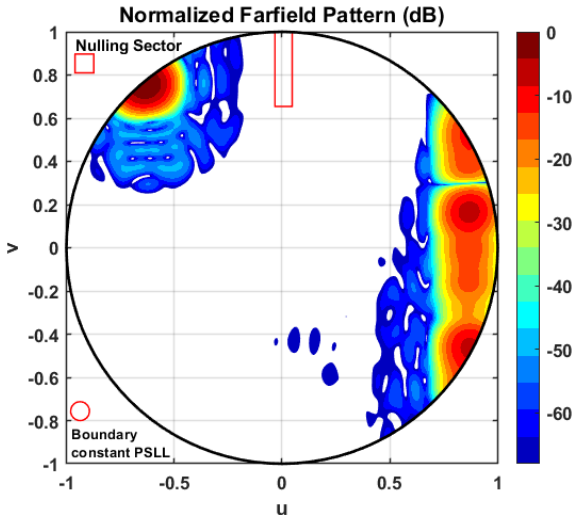

FIGURE 20. Normalized array factor when the main beam is scanned to the angular position $\theta = 80°$, $phi = 130°$ position of the array factor pattern shown in Fig. 17(a). Example 3 of this paper.

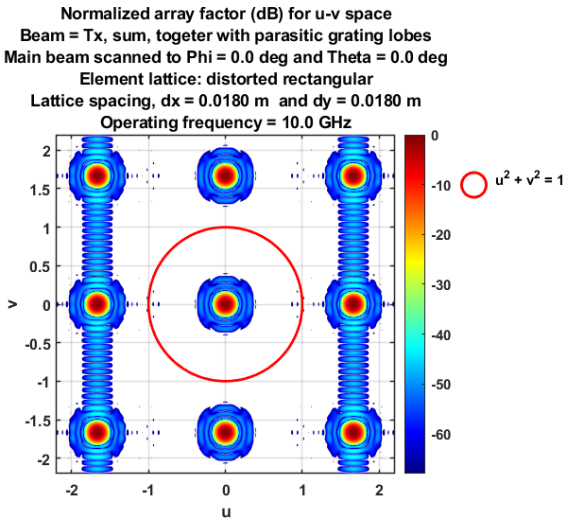

FIGURE 21. Normalized AF of Example 1 in [1].

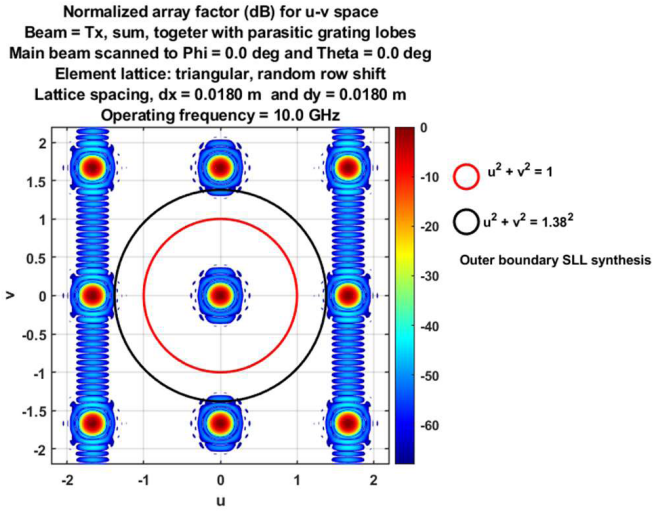

FIGURE 22. Normalized AF of renewed Example 1 of this paper.

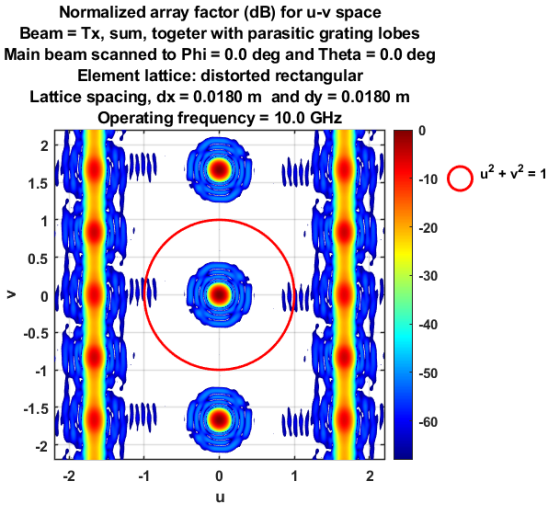

FIGURE 23. Normalized AF of Example 2 in [1].

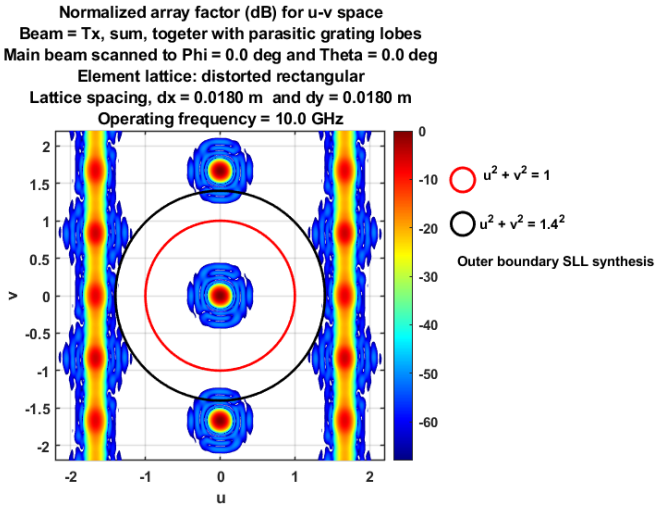

FIGURE 24. Normalized AF of renewed Example 2 of this paper.

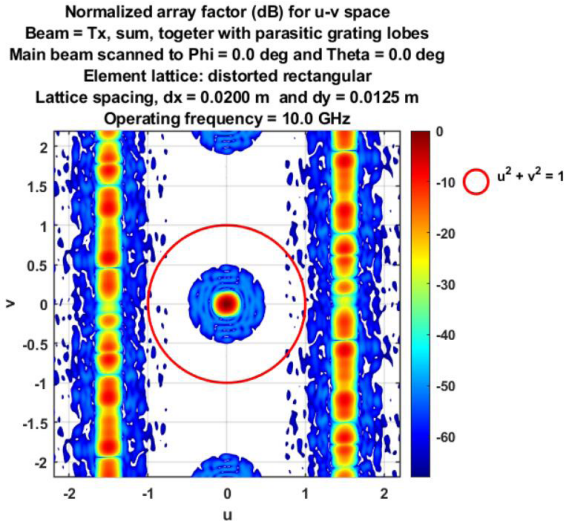

FIGURE 25. Normalized AF of Example 3 in [1].

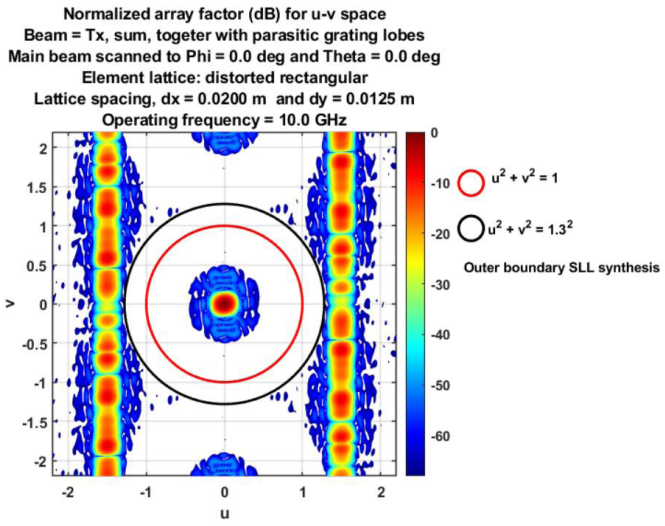

FIGURE 26. Normalized AF of renewed Example 3 of this paper.

TABLE 1. Characteristics original designs and renewed designs.

Example	# of elements	Size aperture	Original Design			Renewed Design		
			Dir (dB)	Beamwidth		Dir (dB)	Beamwidth	
				3 dB_u	3 dB_v		3 dB_u	3 dB_v
1	484	0.4 m x 0.4 m	29.68	0.1118	0.1117	29.55	0.1147	0.1121
2	484	0.4 m x 0.4 m	29.84	0.1094	0.1101	29.79	0.1105	0.1099
3	640	0.4 m x 0.4 m	29.61	0.1158	0.1085	29.33	0.1216	0.1098

TABLE 2. Synthesis execution times original designs and renewed designs.

Example	Original Design		Renewed Design	
	# of iterations	Execution time (s)	# of iterations	Execution time (s)
1	1432	0.99	3436	6.6
2	717	0.43	1922	3.2
3	947	0.76	8800	15.4

to control the involvement of all sidelobes in visible u-v space when synthesizing low sidelobe patterns.

It can be seen from Figs. 21–26 that none of the three examples is suitable for wide angle scanning. However, it cannot be excluded that row displacements can improve the scanning range in one direction as proven in [3, 4] by applying column displacements instead of row displacements. However, from Figs. 21–26 it can be seen that by increasing the number of horizontal row displacements the peak level of the gratings lobes is lowered. The suppression of grating lobes will be addressed in a future publication. In [5] a general analytical method is described to suppress grating lobes for planar arrays with large element spacings.

5. COMPARISON ORIGINAL DESIGNS WITH RENEWED DESIGNS

Table 1 shows the main performance characteristics of the three original synthesized designs of [1] and those of the three revised synthesized designs. This table shows that the differences with respect to directivity and 3 dB beamwidth are very marginal.

Table 2 shows the calculation time required for the IFT synthesis along with the corresponding number of iterations for both the original designs and renewed designs.

6. CONCLUSIONS

The revised pattern synthesis applied to the three examples of [1] show results that fully match the user defined requirements, which is not entirely the case with the published pattern synthesis results in [1]. The single periodicity of *AFuv* in u-v space is responsible for the shortcoming reported in [1] for the synthesized results caused by row displacements. This single periodicity, which only applies to the v-direction of u-v space and not to the u-direction, excludes that all required far-field directions will be involved in the pattern synthesis using the IFT method when the width of *AFuv* is < 2. The pattern synthesis results reported in this paper prove the success of the solution used to eliminate the negative impact of the missing double periodicity on the correct performance of the IFT method. The use of dummy elements at each row with a zero amplitude turned out to be a very effective way to cancel the negative effect of the single periodicity of AF in u-v space.

The described low sidelobe pattern results were performed on a PC with an Intel Core i9-12900K processor and 32 GB RAM. The MATLAB programming language used for the IFT low sidelobe pattern synthesis is version R2024b.

REFERENCES

[1] Keizer, W. P., "Fast low sidelobe pattern synthesis of planar arrays having a distorted triangular or rectangular lattice due to row displacements," *Progress In Electromagnetics Research M*, Vol. 132, 85–94, 2025.

[2] Keizer, W. P. M. N., "Low sidelobe pattern synthesis of array antennas with a triangular or skew lattice using the IFT method," *IEEE Open Journal of Antennas and Propagation*, Vol. 4, 1000–1015, 2023.

[3] Mailloux, R. J., "Wideband quantization lobe suppression in arrays of columns for limited field of view (LFOV) scanning," in *2015 IEEE International Symposium on Antennas and Propaga-*

tion & USNC/URSI National Radio Science Meeting, 2453–2454, Vancouver, BC, Canada, Jul. 2015.

[4] Wang, H., D.-G. Fang, and Y. L. Chow, "Grating lobe reduction in a phased array of limited scanning," *IEEE Transactions on Antennas and Propagation*, Vol. 56, No. 6, 1581–1586, Jun. 2008.

[5] Zeng, Y., X. Ding, X.-L. Ye, F. Costa, G. Manara, and S. Genovesi, "A general analytical arrangement for large-spacing planar scanning array grating lobe suppression based on energy homogenization theory," *IEEE Transactions on Antennas and Propagation*, Vol. 72, No. 9, 7389–7394, Sep. 2024.